Inorganic Chemistry

ARTICLE

pubs.acs.org/IC

Investigation of the First-Order Phase Transition in the $Co_{1-x}Mg_xMoO_4$ Solid Solution and Discussion of the Associated Thermochromic Behavior

L. C. Robertson,[†] M. Gaudon,*[,†] S. Jobic,[‡] P. Deniard,[‡] and A. Demourgues[†]

[†]Université de Bordeaux, CNRS, ICMCB, 87 avenue du Dr. Albert Schweitzer, 33608 F-Pessac Cedex, France

[‡]Institut des Matériaux Jean Rouxel, Université de Nantes, CNRS, 2 rue de la Houssinière, BP 32229, 44322 Nantes Cedex 3, France

Supporting Information

ABSTRACT: A series of compounds of $Co_{1-x}Mg_xMoO_4$ compositions has been prepared by a conventional ceramic route. The members of the whole solid solution exhibit a reversible first-order phase transition which was probed by using thermal expansion and low-temperature reflectivity techniques. Whereas the $\alpha \rightarrow \beta$ transition temperature evolves linearly on warming from 435 to 200 °C with x going from 0 to 0.9, the $\beta \rightarrow \alpha$ transition temperature variation falls down on cooling from −40 °C to −140 °C going from $CoMoO_4$ to $Co_{0.1}Mg_{0.9}MoO_4$ with an asymptotic evolution. The phase transition temperatures have been explained on the basis of a crystal polarization effect under substitution of Mg for Co. Thus, from an applicative point of view, new thermochromic pigments with tunable transition temperatures are here proposed.

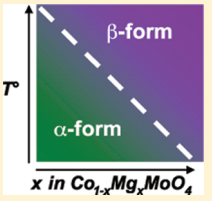

INTRODUCTION

$A^{2+}Mo^{6+}O^{2-}{}_4$ molybdates (A = Co, Ni, Mn, Fe) are widely used as catalyst in selective oxidations.[1−4] The structural features, and more especially the local environment of the A^{2+} and Mo^{6+} cations in the α and β allotropic forms (i.e., the low-temperature or high-pressure and the high-temperature and low-pressure forms, respectively), strongly influence the catalytic behavior of this series of materials. These compounds were also studied for their electronic[5−7] and magnetic properties.[8,9] Moreover, (Co, Ni)MoO_4[1,10,11] and (Co, Fe)MoO_4[12−15] systems received much attention due to their ability to undergo a phase transition. It appears from all these studies that the aforementioned solid solutions were complete and that transition temperatures were composition dependent.

This paper deals with the specific investigation of the $Co_{1-x}Mg_xMoO_4$ series where the substitution of Co^{2+} ($3d^74s^0$ electronic configuration, $rCo^{2+}{}_{HS}$ = 0.745 Å) for Mg^{2+} ($3s^03p^0$ electronic configuration, rMg^{2+} = 0.72 Å) significantly impacts the phase transition temperature. These investigations follow those carried out on the $CuMoO_4$ compound and its W-substituted derivatives where an accurate control of the chemical composition leads to a precise adjustment in temperature of the red (green) to green (red) transition on warming (cooling).[16,17] Such a property may evidently give rise to potential application as an user-friendly temperature indicator of such materials. In that context, $CoMoO_4$ and its Mg derivatives were also studied since the β−$CoMoO_4$ phase is violet and the α−$CoMoO_4$ phase is dark green (see photographs inserted in Figure 2). Due to the strong impact of the Mg rate on the $\alpha \leftrightarrows \beta$ transformation, the Mg substitution appears then as the right parameter to tailor the color change in this family. In the following, the $Co_{1-x}Mg_xMoO_4$ solid solution has been explored on the basis of X-ray diffraction (XRD) analyses. $\beta \rightarrow \alpha$ and $\alpha \rightarrow \beta$ transitions have been probed by reflectivity on cooling and dilatometry on warming, respectively. The origin of the color change as well the evolution of the temperature transition vs x is discussed in terms of the ionocovalency of M−O (M = Mg, Co) and the Mo−O bonds and order−disorder transition.

EXPERIMENTAL SECTION

Synthesis. Pure $Co_{1-x}Mg_xMoO_4$ powders with the β-form were prepared by solid-state reaction from stoichiometric amounts of MoO_3 (Sigma 99.5%), Co_3O_4 (Alfa Aesar 99.7%), and MgO (Cerac Pure 99.95%). Mixture of the reactants was heated in an alumina crucible at 700 °C for 20 h and cooled down to room temperature. The α-form of $Co_{1-x}Mg_xMoO_4$ compounds was obtained at room temperature from their β-form after either manual grinding in an agate mortar or quenching in liquid nitrogen. For Mg-rich samples, a small quantity of β-form may remain whatever the used synthetic route.

Powder X-ray Diffraction. Powder XRD patterns were recorded on a Philips PW 1820 apparatus equipped with a $K\alpha_1/K\alpha_2$ source and a copper anticathode. Diffraction patterns were collected with a 2θ step of 0.02° between 8° and 80° with a counting time of 10s per step in routine mode or, for more advanced investigations, with a 2θ step of 0.008° between 8° and 120° with a counting time of over 200s per step. The patterns have been treated with the Rietveld method (FULLPROF program suite) for the β- and the α-form, the latter being regarded as a subproduct. The diffraction peak profiles were modeled by a pseudo-Voigt function with a Caglioti function for there width. For pattern matching, the refined parameters are the zero shift, the peaks profile parameters U, V, W, and η (Lorentzian/Gaussian distribution), and the unit cell parameters. For Rietveld refinements, atomic positions were fully refined, whereas the occupation rates were fixed from the global composition; moreover, it was decide to fix on each M^{2+} site the

Received: October 14, 2010
Published: March 09, 2011

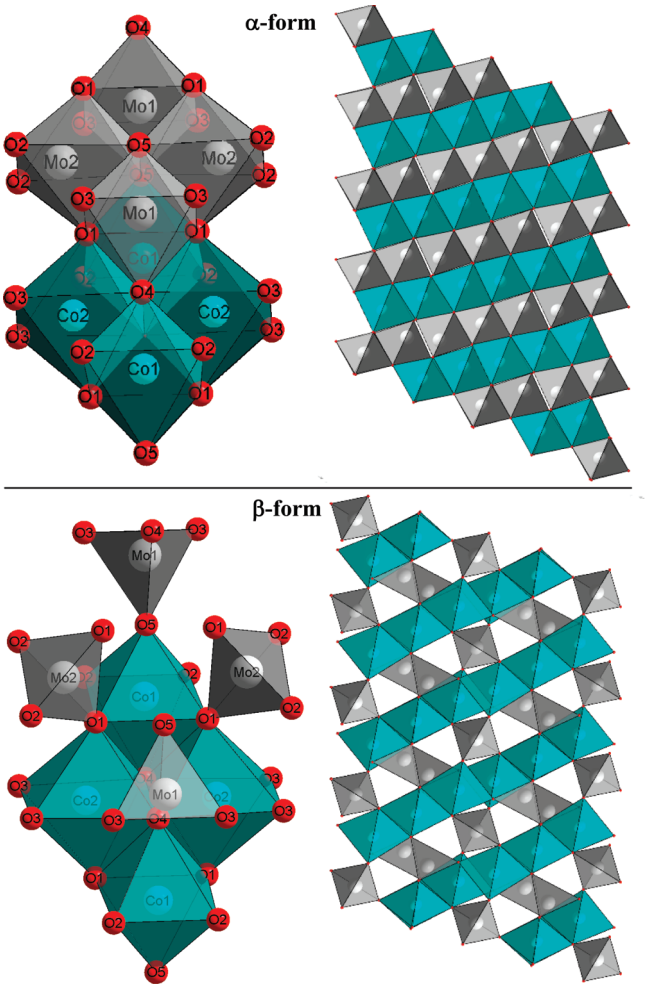

Figure 1. Structure of the α- and β-forms. Left side shows the unit pattern of the structure representation. Right side shows the representation of the unit pattern long distance organization (projection following b axis).

composition ratio between Co^{2+} and Mg^{2+}. The isotropic displacement factors were refined (with a global average value for all oxygen anions).

Reflectivity Measurement. Diffuse reflectance spectra $R(\lambda)$ were recorded at room temperature on a Cary 17 spectrophotometer using an integration sphere in the 350−850 nm wavelength range with a 1 nm step and a 2 nm bandwidth. Halon was used as white reference for the blank.

A home-built instrument equipped with a photomultiplier allowed the collection of the reflected intensity in the 400−680 nm range from 40 °C to −260 °C (cooling rate of about 5 K·min^{-1}).

Thermal Expansion Measurement. The thickness variation vs temperature of α-$Co_{1-x}Mg_xMoO_4$ pellets was recorded on a Netzsch DIL 402C dilatometer in the 25−550 °C temperature range. The pellets were elaborated from β-$Co_{1-x}Mg_xMoO_4$ powdered samples by the application of a 20 MPa uniaxial pressure at room temperature. No presintered treatment was applied to the pellets to avoid any transformation of the α-phase into the β-phase.

RESULTS AND DISCUSSION

Structural Study. All members of the $Co_{1-x}Mg_xMoO_4$ series crystallize in either the α−$CoMoO_4$ or the β−$CoMoO_4$ structure type with $C2/m$ as the space group. In the α-form, both

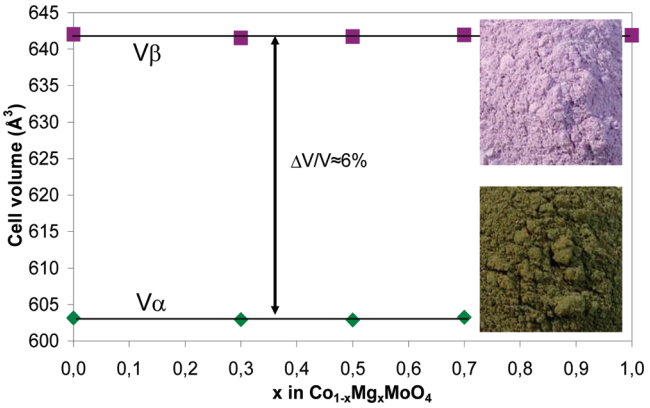

Figure 2. Evolution of cell volume (Å^3) vs x for the α and β-$Co_{1-x}Mg_xMoO_4$ oxides. Photographs of the α- and β-form powders in inset.

Co^{2+} and Mo^{6+} ions occupy distorted octahedral sites. In the β-form, Co^{2+} ions are in distorted octahedral sites, whereas Mo^{6+} cations are 4-fold coordinated to oxygen in distorted tetrahedral sites.[22] The main features of the two crystallographic structures are given in Figure 1. The α-form is built upon octahedra edge-sharing $^2/_\infty[CoO_2]$ and $^2/_\infty[MoO_2]$ layers which condense to give rise a three-dimensional edifice by sharing edges (Figure 1a). These layers consist of $[M_4O_{16}]$ tetramers, constituted by four octahedral sites, connected to each other by the edges. The β-form exhibits $^2/_\infty[CoO_2]$ layers similar to those observed in the α-form, but the layers are connected altogether by isolated tetrahedral $[MoO_4]$ entities (Figure 1b). Thus, the main difference between the two forms consists in the rupture of the one $[Mo_4O_{16}]$ octahedral tetramer in four isolated $[MoO_4]$ tetrahedral sites.

The RT cell parameters for the α and β $Co_{1-x}Mg_xMoO_4$ phases issued from a Rietveld refinement of the XRD patterns are listed in Table 1. The higher observed standard deviations for the α-form than for the β-form may originate from a lower crystalline state of the α-phase compared to the β-phase in relation with the used synthetic route (postgrinding). Furthermore, the α-phase for the extreme composition $MgMoO_4$ cannot be stabilized as main phase from the very incomplete transformation of the β-form into the α-form at room temperature, even after strong grinding, for this composition. On the contrary, the Co-rich compositions exhibit at room temperature before grinding, besides the main β-phase, pollution by α-phase traces. From the difficulty to get pure α- or β-forms and in addition from the low symmetry of the space group ($C2/m$) and the high number of atomic position, the Rietveld refinements lead to poor evaluation of the atomic position (on oxygen ions especially) and quite high R reliability factors. For the five refined compositions (x = 0, 0.3, 0.5, 0.7, 1), the refinement results obtained on the high-temperature (β-)form are shown in the Supporting Information (Tables S1−S5) also with the extracted bond distances (Table S6). The amount of the α-polymorph, when the analyzed sample is biphasic, deduced from Rietveld refinement is given in the Supporting Information tables. For both allotropic forms, the cell parameters and volumes remain roughly constant whatever the magnesium rate (see Figure 2 for the evolution of the cell volume). This was expected from the observation of the ionic radii of Co^{2+} and Mg^{2+} cations in octahedral sites. Notice that volume expansion ($\Delta V/V$) at RT going from α → β-phase is roughly estimated at about +6% for any magnesium rate.[23]

dx.doi.org/10.1021/ic102079f |Inorg. Chem. 2011, 50, 2878–2884

Table 1. Cell Parameters of α-$Co_{1-x}Mg_xMoO_4$ and β-$Co_{1-x}Mg_xMoO_4$ Oxides

x	a(Å)	b(Å)	c(Å)	β(Å)	V(Å^3)
			α-Phase		
0.0	9.716(1)	8.864(1)	7.6769(8)	114.048(7)	603.1(1)
0.3	9.712(3)	8.871(3)	7.657(2)	113.94(3)	602.9(3)
0.5	9.708(7)	8.876(7)	7.649(4)	113.84(5)	602.9(7)
0.7	9.72(1)	8.874(9)	7.648(7)	113.84(8)	603(1)
1.0			no α phase		
			β-Phase		
0.0	10.251(1)	9.294(1)	7.0452(9)	106.962(8)	642.0(2)
0.3	10.2572(6)	9.2911(5)	7.0371(4)	106.949(3)	641.51(6)
0.5	10.2632(4)	9.2922(4)	7.0344(3)	106.949(2)	641.72(5)
0.7	10.2702(6)	9.2919(6)	7.0313(4)	106.918(2)	641.95(7)
1.0	10.2727(4)	9.2905(4)	7.0262(3)	106.888(2)	641.87(4)

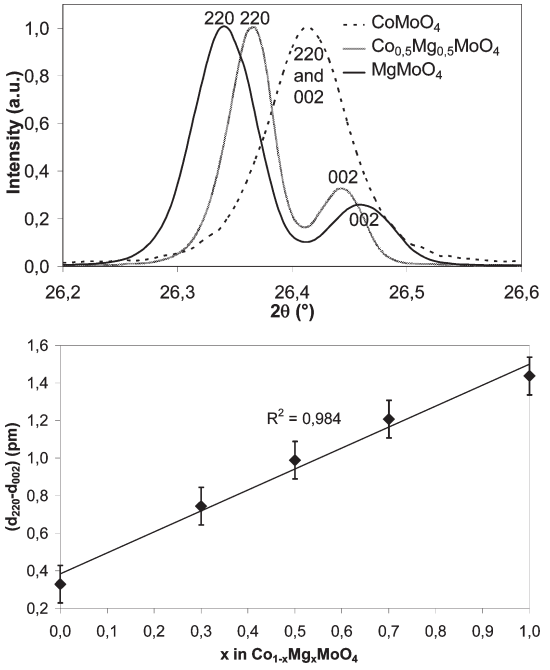

Figure 3. Focus on the (220) and (002) peaks for of the β-$CoMoO_4$ and β-$MgMoO_4$ oxides (top figure) and variation of reticular distance differences associated to (220) and (200) peaks vs magnesium rate (bottom figure).

At this stage we may wonder whether the substitution of Mg for Co lead to a real solid solution, the cell parameters between β-$CoMoO_4$ and $MgMoO_4$ being almost identical. Nevertheless, especially for the β-phase, a slight decrease of the a parameter concomitant with a slight increase of the c parameter with x can be noted. This phenomenon agrees with the existence of a solid solution for the whole $0 \leq x \leq 1$ range, but the cell parameters evolution is so small that a dismutation reaction, as $Co_{1-x}Mg_xMoO_4 \rightarrow (1-x)CoMoO_4 + xMgMoO_4$, cannot be totally rebutted with coexistence of a Co-rich and a Mg-rich phases. However, in addition to the aforementioned cell parameter variation within the β-$Co_{1-x}Mg_xMoO_4$ series, a remarkable difference between the (2θ) positions of the (002) and (220) diffraction peaks can be clearly identified. As shown in Figure 3, the 220 and 002 peaks are superposed for β-$CoMoO_4$, whereas they are separated by 0.15° (2θ scale) for β-$MgMoO_4$. Actually, the plot of the ($d_{220}-d_{002}$) reticular distance difference (see inset) increases linearly with the magnesium rate with a reliability factor close to 1, which constitutes an unambiguous signature of the occurrence of a total solid solution for the β-$Co_{1-x}Mg_xMoO_4$ system.

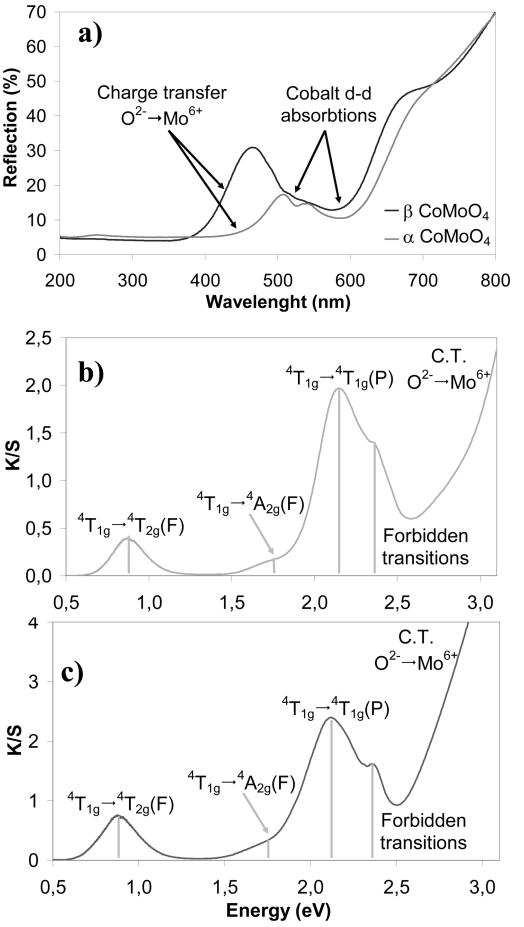

Figure 4. Reflectivity (%) spectra for α and β-$CoMoO_4$ (a) and K/S spectra (Kubelka−Munk transforms) for α-$CoMoO_4$ (b), β-$CoMoO_4$ (c), and Co^{2+} d−d indexation.

UV−vis Properties at Room Temperature. The diffuse reflectance spectra, and their Kubelka−Munk transformation, of α- and β-$CoMoO_4$ compounds, are given in Figure 4a. Both spectra show typical d−d absorption bands assigned to Co^{2+} cations in octahedral sites and an absorption threshold which could be attributed either to an $O^{2-} \rightarrow Co^{2+}$ or a $O^{2-} \rightarrow Mo^{6+}$ charge transfer (CT). Figure 4b and c represents the Kubelka−Munk transformed absorption spectra of the *a*- and *b*-forms, respectively. Based on a d^7 high-spin configuration of Co^{2+} cations, three spin allowed d−d transitions are expected, namely $^4T_{1g} \rightarrow {}^4T_{2g}(F)$, $^4T_{1g} \rightarrow {}^4A_{2g}(F)$, and $^4T_{1g} \rightarrow {}^4T_{1g}(P)$. In fact, three extra bands, very convoluted, can be observed, which are due to forbidden d−d transitions between doublet and quadruplet states as already reported in the literature.[24,25] From the examination of the position in energy of the three allowed transitions, the crystal field intensity (Δ) and the Racah parameter (B) can be calculated using the two equations,

dx.doi.org/10.1021/ic102079f |*Inorg. Chem.* 2011, 50, 2878–2884

Table 2. Three d−d Transition Energies, Crystal Field, and Racah Parameter of the Co^{2+} in α- and *β*-Forms

	α-phase	*β*-phase
$^4T_{1g} \rightarrow {}^4T_{2g}(F)$	0.88 eV	0.84 eV
$^4T_{1g} \rightarrow {}^4T_{1g}(F)$	1.75 eV	1.76 eV
$^4T_{1g} \rightarrow {}^4A_{2g}(P)$	2.12 eV	2.13 eV
Δ_0	0.87 eV	0.92 eV
B	0.082 eV	0.091 eV
Δ_0/B	9.5	9.9

$E_2 - E_1 = 10\Delta$ and $2E_1 - E_3 = 10\Delta - 15B$, where E_1, E_2, and E_3 are the energies of the three aforementioned transitions in the ascending order. Table 2 gathers the energies of the three transitions, the crystal field intensity, and the Racah parameter for both polymorphs. The Δ and *B* parameters are almost not impacted by the nature of the allotropic form. The difference may be probably attributed to the lesser distortion of the $[CoO_6]$ octahedral in the α-form than in the *β*-form.

The position in energy of the CT shifts from visible to UV going from the α- to *β*-phase inducing a severe color change (see photograph). As the Co environment is not significantly impacted by the phase transition, it appears natural to attribute this blue shift to a change in Mo sphere coordination and more specifically to a decrease of the crystal field going from $[MoO_6] \rightarrow [MoO_4]$ building entities. Such a trend has already been discussed in previous studies on $CuMoO_4$ and its W derivatives.[18,21]

Practically, the position of the $O^{2-} \rightarrow Mo^{6+}$ CT moves from 2.4 eV for the α-$CoMoO_4$ to 2.9 eV for the *β*-$CoMoO_4$. The violet color of *β*−$CoMoO_4$ and its Mg derivatives, where the $O^{2-} \rightarrow Mo^{6+}$ charge transfer is located at the UV−vis frontier, is therefore mainly caused by the Co^{2+}d−d absorption bands which range approximately from 650 to 450 nm. The dark-green color of the α-$CoMoO_4$ form and its Mg congeners would be due to the convolution of the Co^{2+} d−d bands and the $O^{2-} \rightarrow Mo^{6+}$ CT; the former giving rise to absorption in the yellow to red wavelengths of the visible spectrum and the latter to absorption of the blue-violet ones.

The evolution of the UV−vis spectrum of *β*-$Co_{1-x}Mg_xMoO_4$ vs *x* is depicted in Figure 5. First, as expected, it can be observed that the intensities of the Co^{2+} d−d transitions decrease when magnesium rate increases. Color shifts progressively from deep to pale violet and white. Moreover, it can be noticed that the CT position is magnesium dependent: Mg^{2+} ions insertion yields a blue shift of the $O^{2-} \rightarrow Mo^{6+}$ charge transfer. In first approximation, this can be explained by considering a network bonds polarization induced by the Mg insertion. Indeed, the electronegativity of Mg is equal to 1.31 (according to Pauling electronegativity scale), whereas that of cobalt is 1.88. Therefore the chemical bonds between magnesium and oxygen are more ionic than between Co and O, and the energy of the $O^{2-} \rightarrow Mo^{6+}$ charge transfer is then increased because the Mo−O bond becomes more covalent on the basis of the competitive bond model. Indeed, the increase of the covalency of the Mo−O bonds via the neighboring of the Mg atoms should induce an increase of the splitting between the bonding and antibonding orbitals descriptive of the Mo−O link. Second, the dependence of the charge-transfer energy vs the Mg rate was analyzed. The charge-transfer energy was determined from the Kubelka−Munk spectrum transformation considering the inflection point (CT_2), the

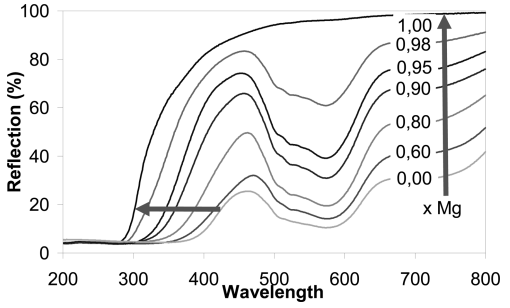

Figure 5. Reflectivity spectra for *β*-$Co_{1-x}Mg_xMoO_4$ with $0.1 \leq x \leq 1.0$.

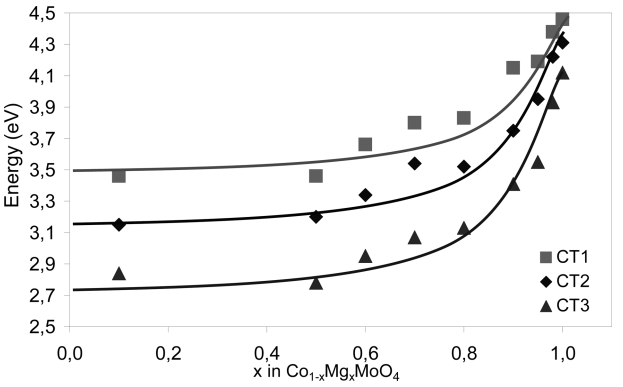

Figure 6. Charge-transfer energies (CT_1, CT_2, and CT_3) vs magnesium rate for *β*-$Co_{1-x}Mg_xMoO_4$ compounds.

end (CT_1), or the beginning (CT_3) of the charge-transfer phenomenon. It was chosen to compare these three characteristic points in order to prevent any systematic error; formally, the d−d Co^{2+} absorption bands being partially convoluted with the $O^{2-} \rightarrow Mo^{6+}$ charge transfer, it can affect the charge-transfer energy determination. Figure 6 displays the evolution of the energy of the various charge-transfer points (CT_1, CT_2, and CT_3) vs magnesium rate. All points exhibit the same evolution: the charge-transfer energy remains roughly constant from *x* equal to 0.1 up to 0.5 and then increases exponentially from the higher *x* values. The nonlinear evolution of the charge-transfer energy with *x* is the consequence of a phenomenon additional to the network polarization. The observed evolution might be explained on the basis of the low third ionization energy for the Co element, considering $Co^{2+}-O^- \leftrightarrow Co^{3+}-O^{2-}$ electronic transfer which may assist the $O^{2-} \rightarrow Mo^{6+}$ charge transfer on the basis of the two $O^{2-}-Mo^{6+} \leftrightarrow Mo^{5+}-O^-$ and $O^-Co^{2+} \leftrightarrow Co^{3+}-O^{2-}$ equilibria. Hence, two cumulative effects operate concomitantly on the $O^{2-} \rightarrow Mo^{6+}$ charge transfer when Mg^{2+} is substituted for Co^{2+} ions: the polarization effect due to Mg^{2+} ions, which increases the $Mo^{6+}-O^{2-}$ bond strength and the charge-transfer energy, and the presence of Co^{2+}, which helps the $O^{2-} \rightarrow Mo^{6+}$ charge transfer due to its low third ionization energy.

Phase Transition Studies. Transition temperatures of $Co_{1-x}Mg_xMoO_4$ phases were determined by means of a UV−vis spectrophotometer for the $\beta \rightarrow \alpha$ low-temperature transition and a dilatometer for the $\alpha \rightarrow \beta$ high-temperature transition. Formally, the use of two distinct techniques was dictated by the very large hysteresis loop associated with the first-order $\alpha \leftrightarrows \beta$ transitions within this series of materials which overlaps on the

dx.doi.org/10.1021/ic102079f |*Inorg. Chem.* 2011, 50, 2878–2884

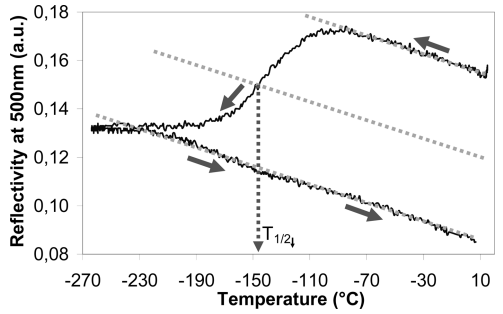

Figure 7. Variation of the reflectivity spectra vs temperature for the $Co_{0.5}Mg_{0.5}MoO_4$ composition and extraction of the $T_{1/2}\downarrow$ temperature.

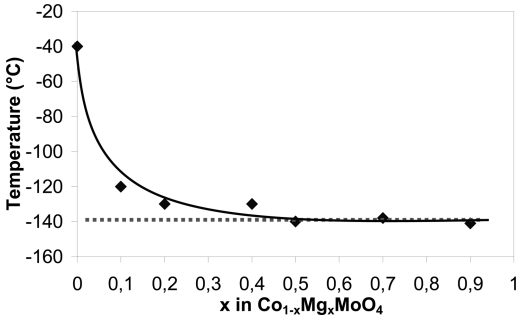

Figure 8. Variation of $T_{1/2}\downarrow$ temperature vs x Mg rate.

temperature ranges accessible by reflectivity and dilatometry at the laboratory. The choice of these two characterization techniques besides thermal differential analyses (TDA), differential calorimetric measurements (DSC), or temperature XRD, which can be also employed, was made because of their ease of access in our laboratory.

The reflectivity at 450 nm of $Co_{0.5}Mg_{0.5}MoO_4$ vs temperature is displayed in Figure 7. Similar curves were collected for $CoMoO_4$, $Co_{0.9}Mg_{0.1}MoO_4$, $Co_{0.8}Mg_{0.2}MoO_4$, $Co_{0.6}Mg_{0.4}MoO_4$, $Co_{0.3}Mg_{0.7}MoO_4$, and $Co_{0.1}Mg_{0.9}MoO_4$. In a first approximation, the $T_{1/2}\downarrow$ temperature corresponds to the 1:1 stoichiometric ratio between the α- and β-phases, i.e., the temperature at which half of the β-phase has been transformed into the α-phase. The evolution of this characteristic temperature vs the Mg content rate is reported in Figure 8, where it appears clearly that the $\beta \rightarrow \alpha$ transition temperature does not follow a linear law. Namely, $T_{1/2}\downarrow$ falls brutally from −40 °C for $CoMoO_4$ to −120 °C for $Co_{0.9}Mg_{0.1}MoO_4$ and then decreases slowly to −140 °C for $Co_{0.1}Mg_{0.9}MoO_4$.

In Figure 9 is given the thermal expansion curve recorded on the $Co_{0.5}Mg_{0.5}MoO_4$ composition. Other compositions give rise to similar curves. Briefly, the expansion curves can be decomposed into three domains: domain I where the sample thermal expansion of the α-form is linear with temperature and not intense (with a thermal expension coefficient of about $7-8 \times 10^{-6}$ K^{-1}); domain II where a brutal dilatation of the pellet associated to the $\alpha \rightarrow \beta$ transition is observed corresponding roughly to 6 vol % of pellet expansion; and domain III for which the sintering is initiated with contraction of the pellet. The $T_{1/2}\uparrow$ was determined as the temperature corresponding to the half of the brutal dilatation associated with the $\alpha \rightarrow \beta$ transition. Figure 10 displays $T_{1/2}\uparrow$ transition temperature vs x. This transition temperature decreases linearly with x.

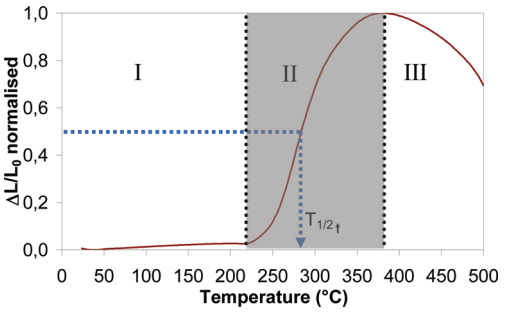

Figure 9. Thermal expansion curve (normalized $\Delta L/L_0$) of the α $Co_{0.5}Mg_{0.5}MoO_4$ pellet and extraction of the $T_{1/2}\uparrow$ temperature.

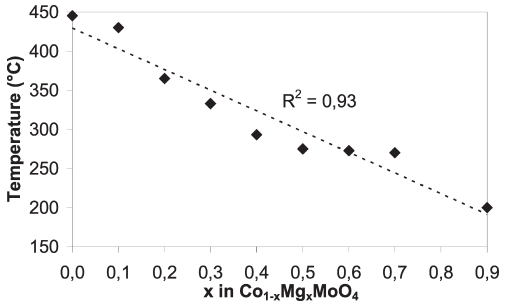

Figure 10. Variation of $T_{1/2}\uparrow$ temperature vs x Mg rate.

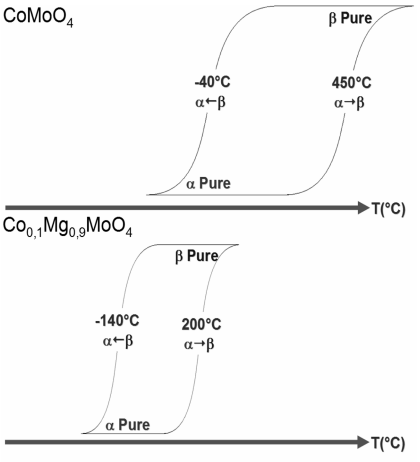

Figure 11. Hysteresis diagrams of $CoMoO_4$ and $Mg_{0.9}Co_{0.1}MoO_4$ compounds.

Table 3. Low-/High-Transition Temperatures and Hysteresis Width of some $Co_{1-x}Mg_xMoO_4$ Compounds

x (Mg)	$T_{1/2}\downarrow$ (°C)	$T_{1/2}\uparrow$ (°C)	ΔT (°C)
0	−40	435	475
0.1	−120	430	550
0.2	−130	365	495
0.4	−130	293	423
0.5	−140	275	415
0.7	−138	270	408
0.9	−141	200	341
1.0		no $\beta \rightarrow \alpha$ transition	

dx.doi.org/10.1021/ic102079f |*Inorg. Chem.* 2011, 50, 2878–2884

The combination of reflectometry and dilatometry measurements made possible the determination of the transition temperatures and the width of the hysteresis loops. Figure 11 represents a schematic view of the hysteresis diagrams for the $CoMoO_4$ and $Co_{0.1}Mg_{0.9}MoO_4$ compositions, while Table 3 sums-up the low- and high-transition temperatures ($T_{1/2}\uparrow$ and $T_{1/2}\downarrow$) and the hysteresis width ($\Delta T_{1/2}$) calculated as the difference between these two transitions temperatures for $Co_{1-x}Mg_xMoO_4$ members with x = 0, 0.4, 0.2, 0.4, 0.5, 0.7, and 0.9.

Based on Table 3, it is worth noticing that a small rate of Mg (around $x = 0.1$) is sufficient to lead to a brutal reduction of $T_{1/2}\downarrow$ ($\beta \rightarrow \alpha$) (from −40 to −120 °C), whereas the $T_{1/2}\uparrow$ ($\alpha \rightarrow \beta$) remains quasi-unchanged in the same composition interval (from 435 to 430 °C). Actually the $T_{1/2}\uparrow$ ($\alpha \rightarrow \beta$) decreases almost linearly with the x Mg rate, whereas the $T_{1/2}\downarrow$ ($\beta \rightarrow \alpha$) decreases sharply and becomes quasi-constant for $x > 0.1$. This surprising behavior is completely different to the one of the $CuMo_{1-x}W_xO_4$ system where the $T_{1/2}\downarrow$ and $T_{1/2}\uparrow$ vary linearly with x in between $CuMoO_4$ and $CuMo_{0.9}W_{0.1}O_4$.[20,21] The occurrence of two strongly different variations of $T_{1/2}\downarrow$ ($\beta \rightarrow \alpha$) and $T_{1/2}\uparrow$ ($\alpha \rightarrow \beta$) as a function of x Mg rate is very unusual and difficult to explain. Thermodynamic (Madelung, interfacial or surface, and strain energies) and kinetic features both influence of the $\alpha \rightarrow \beta$ and $\beta \rightarrow \alpha$ transformation temperatures.

The transformation temperature shifts vs the Mg concentration in $Co_{1-x}Mg_xMoO_4$ solid solution can be rationalized via the bonds polarization variations. As previously explained, on a thermodynamic point of view, the $\alpha \rightarrow \beta$ and $\beta \rightarrow \alpha$ transition temperatures should evolve linearly as a function of the Mg content because of the linear change of the global network polarization vs this Mg content. As Mg concentration increases, the Mg−O ionic bonds tend to create more Mo−O covalent bonds which favor the stabilization of Mo in tetrahedral environment (stabilization of the β-form). However, such a thermodynamic consideration cannot explain the nonlinear $T_{1/2}\downarrow$ ($\beta \rightarrow \alpha$) decrease vs Mg content. A distinctive propagation mode has to be proposed for the specific $\beta \rightarrow \alpha$ half-transition. On the basis of solid-state chemistry considerations, the following explanation can be proposed. In a first approximation, the unusual transition temperature variations vs the chemical composition should be compared to the case of crystal ↔ glass or order ↔ disorder transitions where about the same kinetic behaviors play a key role. On the basis of this consideration, such as order/disorder transition, one can imagine a nonlinear variation of the transition temperatures vs the chemical composition. In our case, the stabilization of the high-temperature form while the Mg^{2+} concentration increases can also be induced by the absence of d electrons for Mg^{2+} cations compared to the Co^{2+} ($3d^7$) one. Indeed, Mg^{2+} cations get a priori a preference for regular octahedral sites and more regular first and second neighbor's environments, as in the β-form. The $\beta \rightarrow \alpha$ transition can hence be viewed as order ↔ disorder transition favored by the Co^{2+} ions. As Mg^{2+} are substituted for Co^{2+} ions, the probability to affect Mo^{6+} second neighbors (one Mg^{2+} impacts six Mo^{6+}) increases rapidly; i.e., the whole crystal distortion is then entirely modified. As a few Mg^{2+} ions are substituted for Co^{2+} ions, the $\beta \rightarrow \alpha$ transition temperature changes drastically and appears at much lower temperatures because the distortion of Mg^{2+} sites, considering the first and the second coordination spheres with the Mg−Mo distances in the α-form becomes very difficult. However, the reverse "ordering effect" occurring for the $\alpha \rightarrow \beta$ half-transition seems to be not impacted and still evolves linearly as a function of the crystal polarization. Then the different behaviors of $T_{1/2}\downarrow$ ($\beta \rightarrow \alpha$) and $T_{1/2}\uparrow$ ($\alpha \rightarrow \beta$) vs x Mg rate observed for the $Co_{1-x}Mg_xMoO_4$ solid solution can be explained on the basis of kinetic features describing the propagation of a local distortion/disorder through a crystal.

CONCLUSION

In this work, the occurrence of a complete solid solution $Co_{1-x}Mg_xMoO_4$ has been demonstrated on the basis of an accurate structural analysis showing the gradual evolution of diffraction lines (2θ position and intensity) as a function of x Mg content, despite that Mg^{2+} and Co^{2+} exhibit the same ionic radii with very closed cell parameters whatever the x Mg rate. The $\beta \rightarrow \alpha$ low-temperature and $\alpha \rightarrow \beta$ high-temperature phase transitions have been investigated on the basis of UV−vis spectra and dilatometry analysis, respectively. The creation of Mg−O ionic bond contributes to generate competitive covalent Mo−O bonds stabilized in tetrahedral coordination in the β-phase and to decrease monotonously the $\alpha \rightarrow \beta$ transition temperature. As far as the $\beta \rightarrow \alpha$ low-temperature transition temperature is concerned, the temperature variation is quite surprising and more difficult to explain. Actually for a few x Mg rate, the $\beta \rightarrow \alpha$ low-temperature transitions drops and remains constant for $x > 0.2$. On the basis of solid-state chemistry approach considering bond polarization, local distortion and disorder as well as kinetics involving order/disorder transition, an explanation of this unusual phenomenon has been proposed. More deep studies by calorimetry with various cooling rates could be performed in order to show the influence of kinetics on the $\beta \rightarrow \alpha$ and $\alpha \rightarrow \beta$ transition temperatures.

ASSOCIATED CONTENT

Supporting Information. five refined compositions (x = 0, 0.3, 0.5, 0.7, 1), the refinement results obtained on the high-temperature (β-)form. α-polymorph, when the analyzed sample is biphasic, deduced from Rietveld refinement. This material is available free of charge via the Internet at http://pubs.acs.org.

AUTHOR INFORMATION

Corresponding Author
*E-mail: gaudon@icmcb-bordeaux.cnrs.fr.

REFERENCES

(1) Barsan, M. M.; Maione, A.; Thyrion, F. C. *Stud. Surf. Sci. Catal.* **2002**, *143*, 1063–1072.
(2) Rodriguez, J. A.; Hanson, J. C.; Chaturvedi, S.; Brito, J. L. *Stud. Surf. Sci. Catal.* **2002**, *130*, 2795–2800.
(3) Brito, J. L.; Barbosa, L. *J. Catal.* **1997**, *171*, 467–475.
(4) Radwan, N. R. E.; Ghozza, A. M.; El-Shobacky, G. A. *Thermochim. Acta* **2003**, *398*, 211–221.
(5) Rodriguez, J. A.; Hanson, J. C.; Chaturvedi, S.; Maiti, A.; Brito, J. L. *J. Chem. Phys.* **2000**, *112*, 935–945.
(6) Rodriguez, J. A.; Chaturvedi, S.; Hanson, J. C.; Albornoz, A.; Brito, J. L. *J. Phys. Chem. B* **1998**, *102*, 1347–1355.
(7) Rodriguez, J. A.; Hanson, J. C.; Chaturvedi, S.; Maiti, A.; Brito, J. L. *J. Phys. Chem. B* **2000**, *104*, 8145–8152.
(8) Sieber, K.; Kershaw, R.; Dwight, K.; Wold, A. *Inorg. Chem.* **1983**, *22*, 2667–2669.
(9) Sleight, A. W.; Chamberland, B. L.; Weiher, J. F. *Inorg. Chem.* **1968**, *7*, 1093–1098.

(10) Maione, A.; Devillers, M. *J. Solid State Chem.* **2004**, *177*, 2339–2349.
(11) Get'man, E. I.; Marchenko, V. I. *Russ. J. Inorg. Chem.* **1980**, *25*, 1072–1074.
(12) Ponceblanc, H.; Millet, J. M. M.; Thomas, G.; Hermann, J. M.; Védrine, J. C. *J. Phys. Chem.* **1992**, *96*, 9466–9469.
(13) Ehrenberg, H.; Svoboda, I.; Wiesmann, M.; Weitzel, H. *Acta Crystallogr.* **1999**, *C55*, 1383–1384.
(14) Domenichi, B.; Vautrein, C.; Pétigny, S.; Bourgeois, S.; Steinbrunn, A. *Mater. Chem. Phys.* **1998**, *55*, 209–214.
(15) Ponceblanc, H.; Millet, J. M. M.; Coudurier, G.; Jegendre, O.; Védrine, J. C. *J. Phys. Chem.* **1992**, *96*, 9462–9465.
(16) Rodriguez, H.; Hernàndez, D.; Garcia-Jaca, J.; Ehrenberg, H.; Weitzel, H. *Phys. Rev. B: Condens. Matter Mater. Phys.* **2000**, *61* (24), 16497–16501.
(17) Hernàndez, D.; Rodriguez, H.; Garcia-Jaca, J.; Ehrenberg, H.; Weitzel, H. *Phys. B (Amsterdam, Neth.)* **1999**, *265*, 181–185.
(18) Thiry, A. E.; Gaudon, M.; Payen, C.; Daro, N.; Létard, J.-F.; Gorsse, S.; Deniard, P.; Roquefelte, X.; Demourgues, A.; Whangbo, M.-H.; Jobic, S. *Chem. Mater.* **2008**, *20*, 2075–2077.
(19) Gaudon, M.; Thiry, A. E.; Deniard, P.; Majimel, J.; Demourgues, A. *Inorg. Chem.* **2008**, *47*, 2404–2410.
(20) Gaudon, M.; Deniard, P.; Demourgues, A.; Thiry, A. E.; Carbonera, C.; Le Nestour, A.; Largeteau, A.; Létard, J.-F.; Jobic, S. *Adv. Mater.* **2007**, *19*, 3517–3519.
(21) Gaudon, M.; Carbonera, C.; Thiry, A. E.; Demourgues, A.; Deniard, P.; Payen, C.; Létard, J.-F.; Jobic, S. *Inorg. Chem.* **2007**, *46*, 10200–10207.
(22) Sleight, A. W.; Chamberland, B. L. *Inorg. Chem.* **1968**, *7*, 1672–1675.
(23) Brown, I. D.; Altermatt, D. *Acta Crystallogr.* **1985**, *B41*, 244–247.
(24) Ravikumar, R.V.S.S.N.; Chandrasekhar, A. V.; Ramamoorthy, L.; Reddy, B. J.; Reddy, Y. P.; Yamauchi, J.; Raoe, P. S. *J. Alloys Compd.* **2004**, *364*, 176–179.
(25) Sreedhar, B.; Sumalatha, Ch.; Yamada, H.; Kojima, K. *J. Non-Cryst. Sol.* **1996**, *203*, 172–175.